Structural Basis for Spinophilin−Neurabin Receptor Interaction†

Matthew S. Kelker,‡ Barbara Dancheck,‡ Tingting Ju,‡ Rene P. Kessler,‡ Jebecka Hudak,‡ Angus C. Nairn,§ and Wolfgang Peti*,‡

Department of Molecular Pharmacology, Physiology and Biotechnology, Brown University, 70 Ship Street, Box G-E3, Providence, Rhode Island 02912, and Department of Psychiatry, Yale University School of Medicine, New Haven, Connecticut 06508

Received November 13, 2006; Revised Manuscript Received December 18, 2006

ABSTRACT: Neurabin and spinophilin are neuronal scaffolding proteins that play important roles in the regulation of synaptic transmission through their ability to target protein phosphatase 1 (PP1) to dendritic spines where PP1 dephosphorylates and inactivates glutamate receptors. However, thus far, it is still unknown how neurabin and spinophilin themselves are targeted to these membrane receptors. Spinophilin and neurabin contain a single PDZ domain, a common protein−protein interaction recognition motif, which are 86% identical in sequence. We report the structures of both the neurabin and spinophilin PDZ domains determined using biomolecular NMR spectroscopy. These proteins form the canonical PDZ domain fold. However, despite their high degree of sequence identity, there are distinct and significant structural differences between them, especially between the peptide binding pockets. Using two-dimensional $^{1}H-^{15}N$ HSQC NMR analysis, we demonstrate that C-terminal peptide ligands derived from glutamatergic AMPA and NMDA receptors and cytosolic proteins directly and differentially bind spinophilin and neurabin PDZ domains. This peptide binding data also allowed us to classify the neurabin and spinophilin PDZ domains as the first identified neuronal hybrid class V PDZ domains, which are capable of binding both class I and II peptides. Finally, the ability to bind to glutamate receptor subunits suggests that the PDZ domains of neurabin and spinophilin are important for targeting PP1 to C-terminal phosphorylation sites in AMPA and NMDA receptor subunits.

Neurabin (*1*) and spinophilin (*2*−*4*) are neuronal scaffolding proteins that play important roles in synaptic transmission and synaptic plasticity (*5*, *6*). Neurabin and spinophilin are highly enriched in dendritic spines, the site of excitatory neurotransmission. Neurabin is expressed almost exclusively in neuronal cells, while spinophilin is expressed ubiquitously, although it is highly enriched in neurons. Because spinophilin is a ubiquitous isoform of neurabin, it is sometimes termed neurabin II (*3*). Neurabin consists of 1095 residues (MW = 122 730 Da), while spinophilin is smaller, consisting of only 817 residues (MW = 89 640 Da). Figure 1a shows a domain representation for both proteins. As is typical for scaffolding proteins, both proteins contain multiple protein interaction domains. Both neurabin and spinophilin contain an F-actin binding, a PP1-binding, a PDZ, and a C-terminal coiled-coil domain. In addition, neurabin, but not spinophilin [in vertebrates (*7*)], contains a sterile α motif (SAM) domain in its C-terminus, while spinophilin, but not neurabin, is proposed to have a dopamine receptor−α-adrenergic interacting domain in its N-terminus, possibly between spinophilin residues 200 and 400 (*8*, *9*). The highest level of primary sequence identity between neurabin and spinophilin is found in the PDZ domains (86%), the protein phosphatase 1 (PP1) binding domains (81%), and the coiled-coil domains (63%).

Both neurabin and spinophilin have a central role in signaling in dendritic spines, as they function to target PP1 toward components of both glutamatergic (fast synaptic transmission) and dopaminergic (slow synaptic transmission) signaling pathways (*10*). Changes in the phosphorylation state of the postsynaptic glutamate receptor α-amino-3-hydroxy-5-methyl-4-isoxazolepropionic acid (AMPA[1])-type channels are important for synaptic plasticity. Regulation of *N*-methyl-D-aspartate (NMDA)-type glutamate receptors also contributes to control of synaptic transmission and plasticity. Protein kinase A (PKA) and calcium/calmodulin-dependent kinase II (CaMKII) play critical roles in phosphorylation and regulation of AMPA receptor trafficking and activity, with PP1 being able to reverse the action of these kinases through

† This work was funded in part by a Richard B. Salomon Faculty Research Award, a Medical Research Grant of the Rhode Island Foundation, and Brown University Start-up Funds to W.P. M.S.K. is supported by NIH-NSRA Fellowship 1F32NS054493-01A1. This material is based upon work supported under a National Science Foundation Graduate Research Fellowship to B.D. R.P.K. is supported by a Karen T. Romer Undergraduate Teaching and Research Award. A.C.N. is supported by grant NIH-MH074866. The ITC instrument was purchased using NSF/EPSCoR funds (Award 0554548).

* To whom correspondence should be addressed. Phone: (401) 863-6084. Fax: (401) 863-6087. E-mail: wolfgang_peti@brown.edu.

‡ Brown University.

§ Yale University School of Medicine.

[1] Abbreviations: NMR, nuclear magnetic resonance; HSQC, heteronuclear single-quantum correlation; rmsd, root-mean-square deviation; AMPA, α-amino-3-hydroxy-5-methylisoxazole-4-propionic acid; NMDA, *N*-methyl-D-aspartic acid; PKA, protein kinase A; CaMKII, calcium/calmodulin-dependent kinase II; DARPP-32, dopamine- and cyclic AMP-regulated phosphoprotein with a relative molecular mass of 32 000 Da; NOE, nuclear Overhauser effect; ITC, isothermal titration calorimetry; PP1, protein phosphatase 1.

10.1021/bi602341c CCC: $37.00
Published on Web 02/06/2007

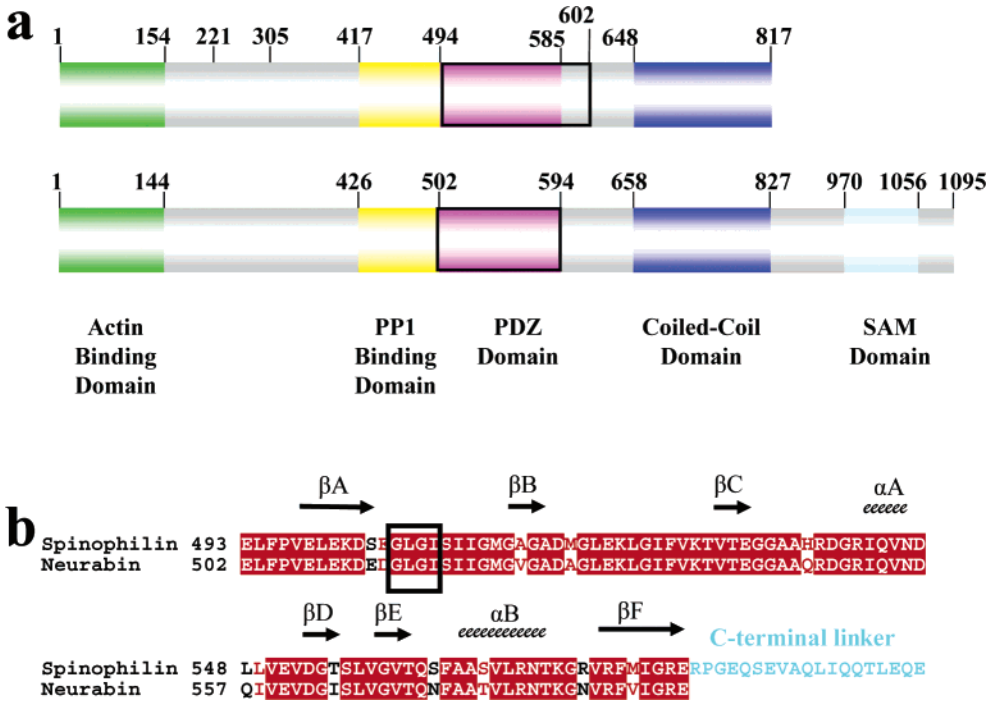

FIGURE 1: Primary amino acid sequences of spinophilin and neurabin. (a) Domain structure of spinophilin (top) and neurabin (bottom). Domains of spinophilin and neurabin studied in this work are highlighted with a black box. (b) Sequence alignment of the spinophilin and neurabin PDZ domains. Experimentally determined secondary structure assignments are annotated as cartoons. The consensus peptide binding sequence, GLGI, is highlighted with a black frame.

its ability to dephosphorylate AMPA receptors. PP1 is also able to dephosphorylate and regulate NMDA receptors (*11*). Through their ability to target PP1 to dendritic spines, neurabin and spinophilin bring the phosphatase into the proximity of AMPA and NMDA receptors. Moreover, localization at dendritic spines allows spatial control of PP1 activity by additional signaling pathways involving D1 dopamine receptor-dependent activation of PKA, activation of the PP1 inhibitor, DARPP-32 (dopamine- and cyclic AMP-regulated phosphoprotein with a relative molecular mass 32 000 Da), and PKA-dependent regulation of the interaction of spinophilin with the F-actin cytoskeleton within dendritic spines (*12*).

PDZ domains, which were originally identified as conserved elements in the postsynaptic density protein PSD-95, the disc-large tumor suppressor Dlg, and the Zonula occludens protein ZO-1, are modular protein interaction domains that recognize and bind C-terminal tetrapeptides from interaction proteins, such as transmembrane receptors (*13*, *14*). They have a critical role in anchoring supramolecular signaling complexes to receptor proteins (*15*). Since PDZ domains mediate binding between large protein−protein assemblies that are involved in signaling and subcellular transport, they have received significant attention as potential drug targets for highly specific signaling pathway regulation (*16*).

All PDZ domains have a conserved Gly-Leu-Gly-Φ binding motif (GLG-Φ, where Φ is a hydrophobic residue and most often is Phe) within the βA and βB connecting loop. This loop is coordinated via a hydrogen bond with the C-terminus of the binding peptide. The binding specificity of PDZ domains is significantly determined by the interaction of the first residue of helix αB and the side chain of residue −2 of the C-terminal ligand. This interaction has resulted in the identification of five distinct classes of PDZ domains (*13*, *16*, *17*). (1) Class I PDZ domains bind peptides with the consensus sequence -X-**S/T**-X-Φ-COOH. The OH group of Ser/Thr forms a hydrogen bond with the class I conserved N3 atom of histidine in helix αB. (2) Class II PDZ domains bind the sequence -X-Φ-X-Φ-COOH (hydrophobic−hydrophobic interaction). (3) Class III PDZ domains bind the sequence -X-**D/E**-X-Φ-COOH, where the acidic residue coordinates with a class III conserved Tyr in helix αB. (4) Class IV PDZ domains bind the sequence -X-Ψ-D/E-COOH, where Ψ is an aromatic residue (*18*, *19*). (5) Class V hybrid PDZ domains are capable of binding both class I type and class II type C-terminal peptides (*20*).

Despite the significant improvement in the detailed physiological understanding of the spinophilin−PP1−DARPP-32−AMPA signaling network (*6*, *21*), extremely limited structural information about the protein interactions that regulate this system is available. Thus, we used biomolecular NMR spectroscopy to elucidate the three-dimensional (3D) structures of the spinophilin and neurabin PDZ domains. Furthermore, we used NMR titration experiments with C-terminal peptides derived from AMPA and NMDA receptors and literature-reported cytosolic interaction proteins to determine if these C-terminal peptides bind the spinophilin and/or neurabin PDZ domains. The results show that spinophilin and neurabin PDZ domains are the first known neuronal class V PDZ domains and that they interact directly with the C-termini of both AMPA and NMDA receptors, interactions that may contribute directly to the ability of PP1 to dephosphorylate closely adjacent C-terminal phosphorylation sites.

MATERIALS AND METHODS

Protein Expression and Purification. Constructs representing spinophilin$_{493-583}$, spinophilin$_{493-602}$, or neurabin$_{502-594}$ were subcloned into a vector derived from pET-28a (Novagen), which encodes a Thio$_6$His$_6$ expression/purification tag (MGSDKIHHHHHH) and a TEV (tobacco etch virus) cleavage site (ENLYFQGH) (*22*). The plasmids were transformed into *Escherichia coli* strain BL21-CodonPlus (DE3)-RIL (Stratagene). The expression of uniformly ^{13}C- and ^{15}N-labeled and ^{15}N-labeled protein was carried out by growing freshly transformed cells in M9 minimal medium containing 4 g/L [^{13}C]-D-glucose and/or 1 g/L $^{15}NH_4Cl$ as the sole carbon and nitrogen sources, respectively. Cell cultures were grown at 37 °C with vigorous shaking to an OD_{600} of 0.6−0.8. The expression of neurabin$_{502-594}$, spinophilin$_{493-583}$, and spinophilin$_{493-602}$ was induced with 1 mM IPTG. The temperature was lowered to 18 °C, and the cell cultures were grown for 18 h. The cells were harvested by centrifugation, resuspended in extraction buffer [10 mM Tris-HCl (pH 8.0), 250 mM NaCl, 5 mM imidazole (pH 8.0), 0.1% Triton X-100, and Complete EDTA free tablets (Roche)], and lysed by cell cracking (Avestin C-3 Emulsiflex). The cell debris was removed by centrifugation (20000*g* for 20 min at 4 °C).

For the first purification step, the soluble proteins were either loaded onto a HisTrap HP column (GE Healthcare), equilibrated with 50 mM Tris-HCl (pH 8.0), 5 mM imidazole, and 500 mM NaCl, or onto a Ni-NTA column (Invitrogen) pre-equilibrated with 10 mM Tris-HCl (pH 8.0), 250 mM NaCl, and 5 mM imidazole (pH 8.0). The protein was eluted with a 5 to 500 mM imidazole gradient. Fractions containing the proteins were pooled and exchanged into a buffer containing 50 mM Tris (pH 7.5) and 50 mM NaCl. After addition of TEV NIa (S219V) protease fused to an in-frame His$_6$ tag, the solutions were incubated at room temperature for 1−3 days. The progression of TEV cleavage was monitored using SDS−PAGE analysis. After cleavage was at least 95% complete, the samples were exchanged into a buffer containing 10 mM Tris-HCl (pH 8.0), 250 mM NaCl, and 5 mM imidazole (pH 8.0) and loaded onto a pre-equilibrated Ni-NTA column (Invitrogen). The flow-through contained only cleaved neurabin$_{502-594}$, spinophilin$_{493-583}$, or spinophilin$_{493-602}$ with an extra N-terminal GHM tripeptide (residues 1−3) as determined by SDS−PAGE. The solution was then concentrated to a final volume of 550 μL. The final concentrations for the different NMR samples were 2 mM for spinophilin$_{493-583}$, 2 mM for spinophilin$_{493-602}$, and 1.5−3 mM for neurabin$_{502-594}$ [20 mM sodium phosphate (pH 6.5), 50 mM NaCl, and 10% D_2O] (*23*).

Most NMR measurements were performed at 298 K on a Bruker AvanceII 500 MHz spectrometer using a TCI HCN z-gradient cryoprobe. Some experiments for neurabin$_{502-594}$ were conducted on a Bruker DRX 600 MHz spectrometer using a room-temperature TXI HCN z-gradient probe. Proton chemical shifts were referenced to internal 3-(trimethylsilyl)-1-propanesulfonic acid, sodium salt (DSS). Using the absolute frequency ratios, the ^{13}C and ^{15}N chemical shifts were referenced indirectly to DSS.

Chemical Shift Assignment and Structure Calculation. The following spectra were used to achieve the sequence-specific backbone and side chain assignments of all aliphatic residues: two-dimensional (2D) ^{1}H−^{15}N HSQC, 2D ^{1}H−^{13}C HSQC, 3D HNCACB, 3D CBCA(CO)NH, 3D CC(CO)NH, 3D HNCO, 3D HNCA, 3D HBHA(CO)NH, 3D ^{15}N-resolved ^{1}H−^{1}H TOCSY, and 3D HC(C)H-TOCSY (*24*). The 2D ^{1}H−^{1}H NOESY, 2D ^{1}H−^{1}H TOCSY, and 2D ^{1}H−^{1}H COSY spectra of the spinophilin$_{493-602}$ and neurabin$_{502-594}$ samples in D_2O solution after complete H−D exchange of the labile protons were used for the assignment of the aromatic side chains. The NMR spectra were processed with Topspin1.3 (Bruker, Billerica, MA) and analyzed with the CARA software package (www.nmr.ch).

For the 3D structure determination of neurabin$_{502-594}$ and spinophilin$_{493-602}$, we used established NMR methods for the sequence-specific backbone and side chain assignments (*24*). Semiautomated programs were used to evaluate the data (CARA). We used the following spectra for the structure calculation: 3D ^{15}N-resolved ^{1}H−^{1}H NOESY, 3D ^{13}C-resolved ^{1}H−^{1}H NOESY (mixing time of 85 ms), and 2D ^{1}H−^{1}H NOESY (mixing time of 85 ms, D_2O solution). NOESY peak picking, NOESY peak assignment, and 3D structure calculation were performed automatically, using the ATNOS/CANDID/CYANA software package (*25*−*27*). The inputs for the structure calculations of the neurabin and spinophilin PDZ domains were amino acid sequences, the complete chemical shift lists, and the 3D and 2D NOESY spectra. Constraints for backbone dihedral angles derived from ^{13}C chemical shifts were used only in the initial structure calculation. In a second step, the automatically picked NOESY peak lists were manually improved and used as input for the CYANA program package, which was used for the final structure calculation. This additional manual step improved the quality of the structures substantially. Our experience shows that the ATNOS/CANDID approach works optimally with high-field NOESY spectra recorded at 800 and 900 MHz because of an improved resolution and signal to noise ratio (*28*−*30*). However, when this additional manual step is performed, NOESY spectra recorded at lower field, like ours at 500 MHz, can also be used successfully.

A total of 2217 NOESY-derived distance constraints (∼24 NOE constraints per residue) were used for the structure calculation of neurabin$_{502-594}$ and 1507 (∼14 NOE constraints per residue) for spinophilin$_{493-602}$. The decrease in the number of NOE constraints per residue for spinophilin compared to neurabin is easily ascribed to the 19-residue highly flexible C-terminal linker in spinophilin, for which very few NOE constraints were found and which increased the number of unresolved peaks in the 2D and 3D NOESY spectra (Table 1). The recently reported RECOORD scripts, in conjunction with CNS, were used for energy refinement in a water shell (*31*, *32*). The neurabin$_{502-594}$ model has excellent stereochemistry, with 98.6% of the residues in the most favored and additionally allowed regions of the Ramachandran diagram, 1% in the generously allowed region, and 0.4% in the disallowed region. Similarly, for spinophilin$_{493-602}$, 97.5% of the residues are in the most favored and additionally allowed regions, 1.6% in the generously allowed region, and 0.9% in the disallowed region. Again, the lower stereochemical quality of the spinophilin PDZ domain structure, determined by a 1.1% increase in the percentage of residues in the generously allowed and disallowed regions of the Ramachandran plot, is due to increased spectral overlap and the lack of detectable long-range NOEs in the largely unstructured C-terminal

Table 1: Structural and CNS Refinement Statistics

	spinophilin$_{493-602}$	neurabin$_{502-594}$
no. of restraints		
unambiguous distance restraints (all)	1507	2217
intraresidual	437	474
sequential	471	618
medium-range	208	378
long-range	391	747
deviations from idealized covalent geometry		
bonds (Å)	0.012 ± 0.0003	0.013 ± 0.0005
angles (deg)	1.32 ± 0.033	1.33 ± 0.034
impropers (deg)	1.56 ± 0.11	1.53 ± 0.09
structural quality		
Ramachandran plot [NMR-PROCHECK (*34*)]		
most favored region (%)	73.0	77.4
additionally allowed region (%)	24.5	21.2
generously allowed region (%)	1.6	1.0
disallowed region (%)	0.9	0.4
pairwise rmsd (Å)		
backbone (N, C$^{\alpha}$, C, and O) (4−25, 35−93)	0.88 ± 0.18	0.58 ± 0.11
all heavy atoms (4−25, 35−93)	1.41 ± 0.2	1.25 ± 0.17

Table 2: C-Terminal Peptides Derived from AMPA and NMDA Receptors and Literature-Reported Interaction Proteins

receptor	protein	peptide	PDZ class	k_{ex}[a]	interaction surface[b]
AMPA	GluR1	GATGL	I		
	GluR2	ESVKI	II	$\gg 10^4$	small
	GluR3	GTESVKI	II	$\gg 10^4$	small
	GluR4	ASDLP			
NMDA	NR1C2	SRHRES			
	NR1C2′	SVSTVV	I	$\gg 10^4$	large
	NR2A/B	SIESDV	I	$\gg 10^4$	large
	NR2C/D	SLESEV	I	$\gg 10^4$	large
	NR3A	NRTCES			
	NR3B	AAPAES			
	AM-NR hybrid	ESVKV	II	$\gg 10^4$	large
	P70S6 Kinase	EHLRMNL	II	10^2-10^4	small
	Kalirin−7	DPFSTYV	I	10^2-10^4	large

[a] k_{ex} is the estimated peptide−protein exchange constant (*51*, *52*). [b] Interaction surface correlates with the number of residues involved in complex formation (Figure 6).

linker tail of the spinophilin$_{493-602}$ PDZ domain. The chemical shift assignment of the spinophilin PDZ domain has been recently published (*23*). The quality of the structures was assessed with WHATCHECK (*33*), AQUA (*34*), NMR-PROCHECK (*34*), and MOLMOL (*35*). All structure comparisons throughout this work were performed using the closest conformer to the mean structure for all PDB entries.

Peptide Library Screening. Peptide ligands derived from the C-terminus of NMDA and AMPA channels and cytosolic proteins [P70 S6 kinase (*36*) and kalirin-7 (*37*)] are listed in Table 2. Peptides were obtained at >95% purity either from JPT Peptide Technologies Inc. or from the Keck Foundation Biotechnology Resource Laboratory at Yale University. All peptides were solubilized in the same buffer that was used for the NMR measurements of the PDZ domains. The NR1C2′ peptide (SVSTVV) was the only peptide not soluble in this buffer and was solubilized by DMSO. DMSO without the NR1C2′ peptide was added to the neurabin and spinophilin PDZ domains and a 2D ^{1}H−^{15}N HSQC spectrum recorded to ensure no interaction of DMSO with the PDZ domains (Figure S4 of the Supporting Information). Interaction study measurements were carried out on a Bruker AvanceII 500 MHz spectrometer equipped with a TCI HCN z-gradient cryoprobe. A 2D ^{1}H−^{15}N HSQC spectrum was used to monitor perturbations in ^{1}H and ^{15}N chemical shifts, which occur due to peptide binding. Comparison of the bound and unbound 2D ^{1}H−^{15}N HSQC spectra was used to detect binding using TopSpin1.3 (Bruker). Data were analyzed using the CARA software package (www.nmr.ch).

We calculated dissociation constants (K_d) from the NMR chemical shift perturbation measurements. Chemical shift resonances of spinophilin/neurabin PDZ domains that exhibited the most significant change upon peptide interaction (GLGΦ binding motif, βB, αB) and, in addition, were well-resolved were used for these calculations. The averaged proton and nitrogen chemical shift changes $[\sqrt{(\delta_H-\delta_0)^2+(\delta_N-\delta_0)^2}]$ were fitted to the following standard equation using the nonlinear regression analysis package of Mathematica 5.2 (Wolfram Research Inc.):

$$\delta = \delta_m \frac{[m_0 + p_0 + K_d - \sqrt{(m_0 + p_0 + K_d)^2 - 4m_0p_0}]}{2m_0}$$

where m_0 and p_0 are the initial concentrations of the PDZ domain and the peptide, respectively, δ_m is the maximum chemical shift change for the protein−peptide complex (1:5 or 1:10 measurements), and K_d is the dissociation constant. In addition, we used isothermal titration calorimetry (ITC) measurements using a Microcal (Northampton) VP-ITC microcalorimeter to confirm the K_d values obtained using NMR data analysis (Table S1 of the Supporting Information). Since ITC measurements for protein−peptide interaction studies with K_d values in the low micromolar range, the typical range expected for PDZ−peptide interactions, require a large amount of protein and peptide, only a selective experiment was conducted to confirm the NMR titration results.

Chemical Shift Assignments and Coordinates. Chemical shift assignments of neurabin$_{502-594}$ were deposited in the BMRB as entry 6933, and coordinates were submitted to the Protein Data Bank as entry 2FN5. Chemical shift assignments of spinophilin$_{493-602}$ were deposited in the BMRB as entry 6927, and coordinates were submitted to the Protein Data Bank as entry 2G5M.

RESULTS

Structural Analysis

3D Structures of the Neurabin and Spinophilin PDZ Domains. Two constructs for the spinophilin PDZ domain and one construct for the neurabin PDZ domain were expressed and purified. The first of these constructs is spinophilin$_{493-583}$, which comprises the spinophilin PDZ domain, and the second is spinophilin$_{493-602}$, which comprises the spinophilin PDZ domain and a 19-amino acid C-terminal extension that functions as a linker to the C-terminal coiled-coil domain (Figure 1A,B; Figure S1 of the Supporting Information). Secondary structure prediction programs (*38*) predict that this linker may form an α-helix. By comparison of the 2D ^{1}H−^{15}N HSQC spectra of both constructs, 16

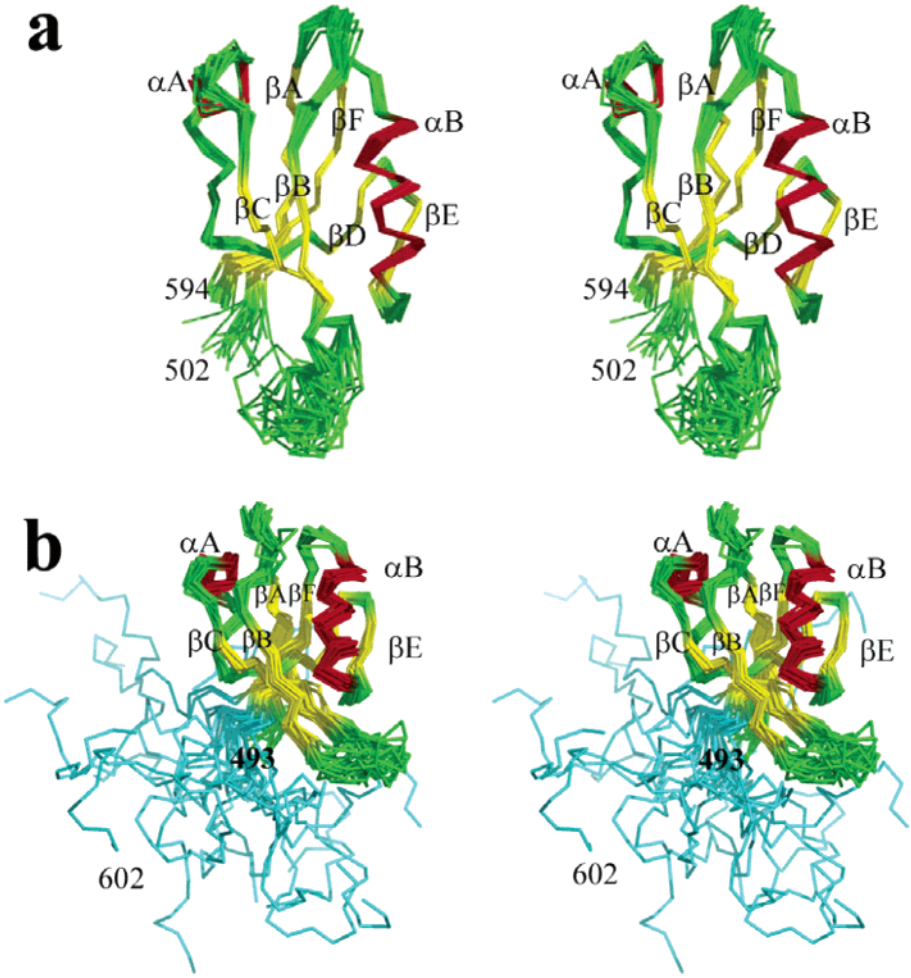

FIGURE 2: NMR structures of (a) neurabin$_{502-594}$ and (b) spinophilin$_{493-602}$ Cα polypeptide backbone chains of a bundle of 20 energy-minimized conformers superimposed for minimal rmsd values of the backbone atoms of residues 504−529 and 539−590 in neurabin and corresponding residues in spinophilin. The C-terminus of spinophilin$_{493-602}$ is disordered (turquoise correlating to turquoise residues in Figure 1B). α-Helices are colored red, *β*-strands yellow, and all residues not in regular secondary structural elements green. Secondary structural elements are labeled following common PDZ domain nomenclature. The PDZ domain binding pocket is flanked by *β*-strand *β*B and helix αB. The numbers 502 and 594, and 483 and 602, identify the N- and C-termini for neurabin and spinophilin, respectively. This figure and all subsequent figures were generated using PyMOL (*53*).

additional cross-peaks were identified in the 2D $^{1}H-^{15}N$ HSQC spectrum of spinophilin$_{493-602}$. These 16 additional cross-peaks correlate well with the 19-amino acid extension of this construct. Importantly, the chemical shift pattern of the spinophilin PDZ domain, identified by overlap of the 2D $^{1}H-^{15}N$ HSQC spectrum of spinophilin$_{493-602}$ with that of spinophilin$_{493-583}$, exhibited identical $^{1}H-^{15}N$ chemical shifts (except the last three C-terminal residues now extended by the 19-residue linker), demonstrating that the 3D structure of the spinophilin PDZ domain is not influenced by the C-terminal linker. Therefore, the structure of spinophilin$_{493-602}$ was elucidated to determine whether there is residual structure in the linker region. In addition, the structure of the neurabin PDZ domain, neurabin$_{502-594}$, without this C-terminal linker was elucidated, to characterize potential structural differences between the spinophilin and neurabin PDZ domains.

The Extended C-Terminal Loop of Spinophilin Is Unstructured. As expected, the neurabin$_{502-594}$ and spinophilin$_{493-602}$ structures form typical PDZ folds (Figure 2). The 3D structures of the neurabin and spinophilin PDZ domains, like most PDZ domains, are comprised of six *β*-strands, *β*A−*β*F, and two α-helices, αA and αB. These secondary structure elements fold into a six-stranded *β*-sheet flanked by the two α-helices. The C-terminal recognition peptide binding groove is located between the *β*B strand and the αB helix.

Notably, no secondary structure, based on chemical shift indexing and $H^{N}-H^{N}$ NOE analysis, was determined in the C-terminal extension of spinophilin$_{493-602}$. Instead, the 19-residue C-terminal extension appears to be highly flexible, based on its increased intensity of N^{H} cross-peaks (increased transverse relaxation time) in the 2D $^{1}H-^{15}N$ HSQC spectrum and dramatically reduced numbers of cross-peaks in the 3D ^{15}N-resolved $^{1}H-^{1}H$ NOESY spectrum when compared to N^{H} cross-peaks from the rest (core PDZ domain) of the protein. Outside of this linker, the most notable difference between the two PDZ domains is that the loop between *β*B and *β*C of spinophilin is angled toward and cradles the αB helix, whereas in the neurabin structure, it does not (Figures 2 and 3). There are five glycine and two alanine residues in the *β*B and *β*C loop region which likely contribute to its high conformational flexibility. Thus, it seems that the highly mobile 19-residue C-terminal tail of spinophilin, which occupies a large amount of steric space, constrains this loop to the observed more bent conformation.

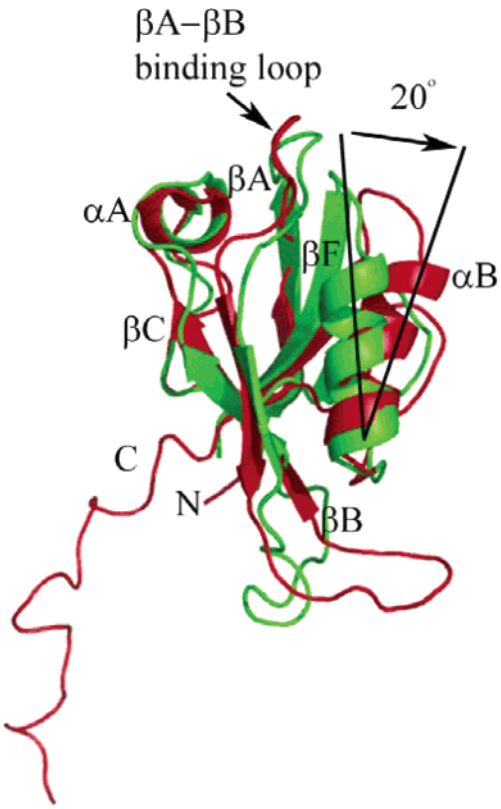

FIGURE 3: Comparison of the 3D structures of the neurabin (green) and spinophilin (red) PDZ domains determined in this study. Core residues with a rmsd of <1 Å were superpositioned to illustrate the tilt of helix αB between the neurabin and spinophilin PDZ domain structures. The global rmsd between the two structures is 1.74 Å, including all main chain atoms, excluding the highly mobile loop region between β-strands βB and βC (residues 518−528 in spinophilin). Black lines along αB form an ~20° angle separation between this helix between the structures. This comparison was done using the energy-minimized conformer of the spinophilin and neurabin PDZ domain structures that is closest to the mean structure of these PDZ domains.

After we determined the structure of neurabin$_{502-594}$, the Japanese Riken Structural Genomics Consortium released the coordinates for a second construct of this domain, residues 501−594, which includes seven N-terminal and six C-terminal residue cloning artifacts (PDB entry 1WF8). The PDB file refers to this domain as the spinophilin PDZ domain. However, by primary sequence analysis, it is clear that this is actually the neurabin PDZ domain. The rmsd between the two average neurabin NMR structures is 1.4 Å over 78 residues (84% of the total which excludes the large flexible loop between βB and βC, but includes all other loop regions), indicating a high degree of similarity between the two structures. Notably, the seven N-terminal and six C-terminal residue cloning artifacts are highly flexible, similar to what is observed for the C-terminal linker in the spinophilin PDZ domain. Also here, βB and βC are pushed more toward the αB helix following our spinophilin PDZ domain model.

In Spite of an 86% Level of Sequence Identity, the Structures of the Spinophilin and Neurabin PDZ Domain Are Not Identical. The root-mean-square deviation (rmsd) between the spinophilin and neurabin PDZ domains is 1.74 Å, which includes all main chain residues except for the highly mobile βB−βC loop. In Figure 3 (red for spinophilin and green for neurabin), a subset of residues of both PDZ domains were overlapped to achieve a rmsd of <1 Å, aiding the visual distinction of major structural differences between the two proteins. The βA−βB loop of neurabin, which contains the highly conserved C-terminal binding motif, GLG-Φ, is tilted toward the ligand binding site compared to that of spinophilin. In addition, the αB helix of neurabin is also tilted inward toward the peptide binding pocket, whereas the helix of spinophilin is not, resulting in an ~20° different orientation of the helices. This results in a narrowing of the neurabin peptide binding pocket compared to spinophilin. This differential arrangement of the βA−βB loop region and the αB helix of neurabin and spinophilin is due to two single-amino acid substitutions. First, Arg575 in spinophilin is substituted with Asn584 in neurabin (Figures 1B and 4 and Figure S1 of the Supporting Information). In spinophilin, the side chain of Arg575 forms a bipartite salt bridge with the side chain of Glu500. The long arginine side chain pushes the loop between helix αB and the last β-strand, βF, away from the ligand binding pocket and also from β-strand βA (which is shorter then βA in neurabin). This gives rise to the more pronounced tilt of helix αB in the spinophilin PDZ domain. Second, Thr555 in the spinophilin PDZ domain is substituted with Ile564 in the neurabin PDZ domain (Figure S2 of the Supporting Information). In neurabin, the much more bulky isoleucine side chain exhibits a strong steric constraint in the interaction with Val577 in helix αB. The dramatically decreased bulkiness (Ile to Thr substitution) of the Thr555 and Val568 interaction in the spinophilin PDZ domain leads to a more open peptide binding pocket for the spinophilin PDZ domain.

The Spinophilin Peptide Binding Pocket Is More Basic than That of Neurabin. Electrostatic surface potential maps were generated to compare the molecular surfaces of neurabin and spinophilin (Figure 5). The predicted pI values of neurabin$_{502-594}$, spinophilin$_{493-583}$ (PDZ domain only), and spinophilin$_{493-602}$ (PDZ domain and linker) are 4.63, 5.11, and 4.78, respectively. These small differences are evident in the calculated electrostatic surface potential distribution. Specifically, spinophilin contains more basic patches than neurabin. Most importantly, the peptide binding pocket of neurabin is relatively neutral compared to the larger basic patch in spinophilin. This change cannot be explained by a leucine to glutamine substitution at position 550 of the spinophilin PDZ domain. Instead, this basic patch is again created indirectly by Arg575 in spinophilin: in the neurabin PDZ domain structure, the side chain of Lys582 forms a salt bridge with the side chain of Asp562. In spinophilin, the bulky side chain of Arg575 pushes the side chain of Val576 away from its original position to form a hydrophobic patch with Phe578. This disrupts the formation of the Lys−Asp salt bridge that is present in the neurabin PDZ domain, pushing the lysine residue toward the binding pocket and creating this positively charged patch.

Peptide Interaction Studies

The Spinophilin and Neurabin PDZ Domains Are the First Experimentally Confirmed Neuronal Class V PDZ Domains. It is not possible to predict the PDZ domain class to which a PDZ domain belongs from either its sequence or structure, since the class is defined by the sequence of the interacting peptides. Thus, we used C-terminal peptides, derived from receptors and cytosolic proteins, to investigate which peptides

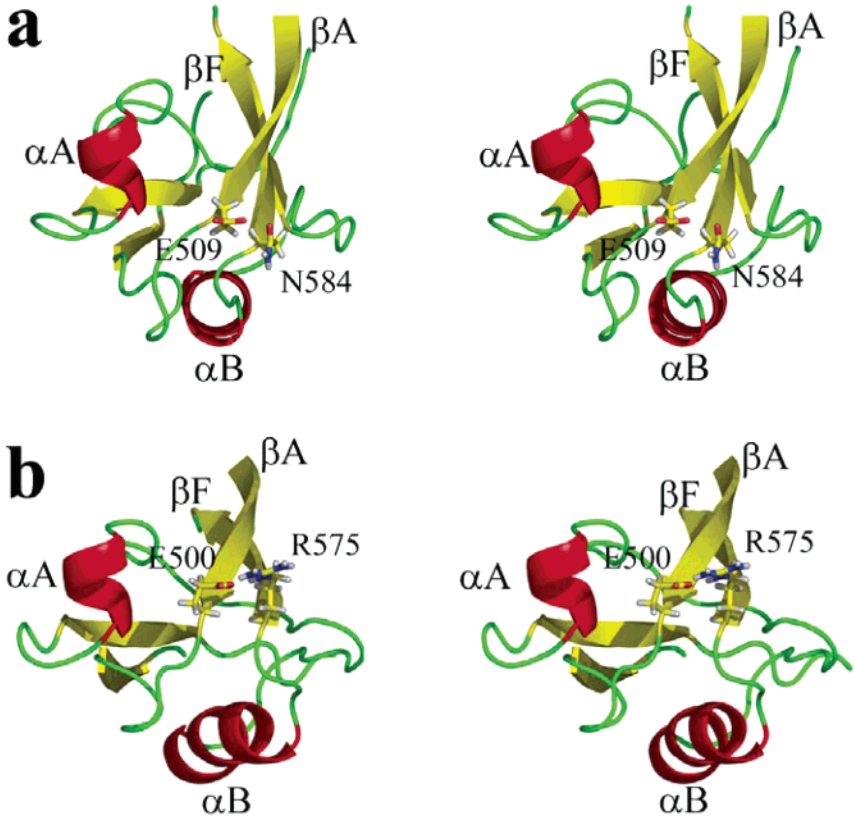

FIGURE 4: Top view of (a) neurabin$_{502-594}$ and (b) spinophilin$_{493-602}$. Structures are superpositioned on helix αA. In spinophilin, Arg575 forms a salt bridge with Glu500. The corresponding residue in neurabin, Asn584, does not form this salt bridge. The resulting shortening of βA and βF and the tilt of αB are shown.

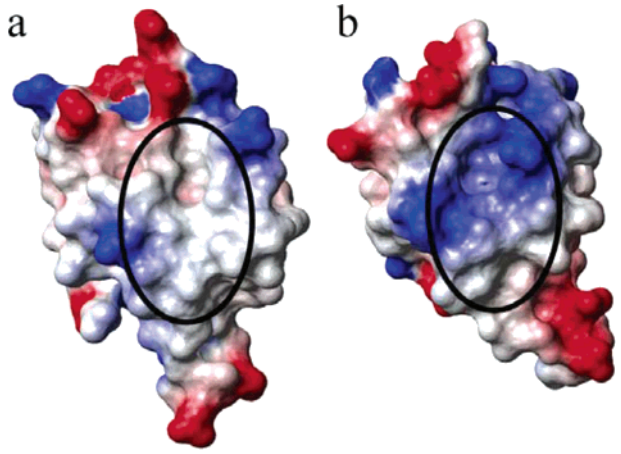

FIGURE 5: Electrostatic surface potential of the (a) neurabin and (b) spinophilin PDZ domains. The 19-residue C-terminal, highly mobile tail of the spinophilin PDZ domain has been omitted for clarity. The electrostatic surface potentials were generated via MOLMOL (*35*). Positive potential is blue, neutral potential white, and negative potential red. The peptide binding site is marked with an oval, illustrating a clear increase in the electropositivity of the ligand binding pocket of the spinophilin PDZ domain.

bind the spinophilin and neurabin PDZ domains. An overview of the screened peptides is given in Table 2. Our results, reported in detail below, have allowed us to classify these PDZ domains as class V PDZ domains and, in addition, provided critical insights into their functional roles for PP1 targeting.

We carried out NMR-based peptide screening using low micromolar concentrations (150 μM) of ^{15}N-labeled spinophilin and neurabin PDZ domains with a 5-fold molar excess of peptide (an example is shown in Figure S3 of the Supporting Information). Peptide binding was assessed by comparing H^N and N chemical shifts between 2D $^1H-^{15}N$ HSQC spectra of the free and bound PDZ domains; differences in the chemical shifts were indicative of PDZ domain−peptide binding. For peptides that bound, we then systematically varied the protein:peptide ratios (1:1, 1:2.5, 1:5, and, for some samples, 1:10 protein:peptide concentration ratios) to determine the binding affinities for each peptide. Using chemical shift changes (see Materials and Methods), we show that the binding affinities of the spinophilin and neurabin PDZ domains for the AMPA and NMDA receptor-derived peptides are in the low micromolar range (2−10 μM). These affinities were then confirmed by ITC measurements. In addition, we observed in the NMR measurements that all receptor-derived peptides that bind the spinophilin and neurabin PDZ domains are in a fast exchange time regime. Thus, these peptide binding experiments demonstrate that spinophilin and neurabin PDZ domains interact directly with C-terminal peptides derived from GluR2, GluR3 (AMPA), and NR1C2′, NR2A/B, NR2C/D (NMDA) receptor subunits. We were unable to detect binding of the neurabin and spinophilin PDZ domains to GluR1, GluR4, NR1C2, and NR3A/B receptor C-terminal peptides.

C-Terminal AMPA receptor-derived binding peptides GluR2 and -3 are PDZ class II binding peptides **(SVKI)**, while NMDA receptor-derived binding peptides NR1C2′, NR2A/B, and NR2C/D are PDZ class I binding peptides (E**S**/**T**X**V**, where X = V, D, or E). Therefore, both the spinophilin and neurabin PDZ domains are class V PDZ domains, which can bind both class I and class II type peptides (*20*). These

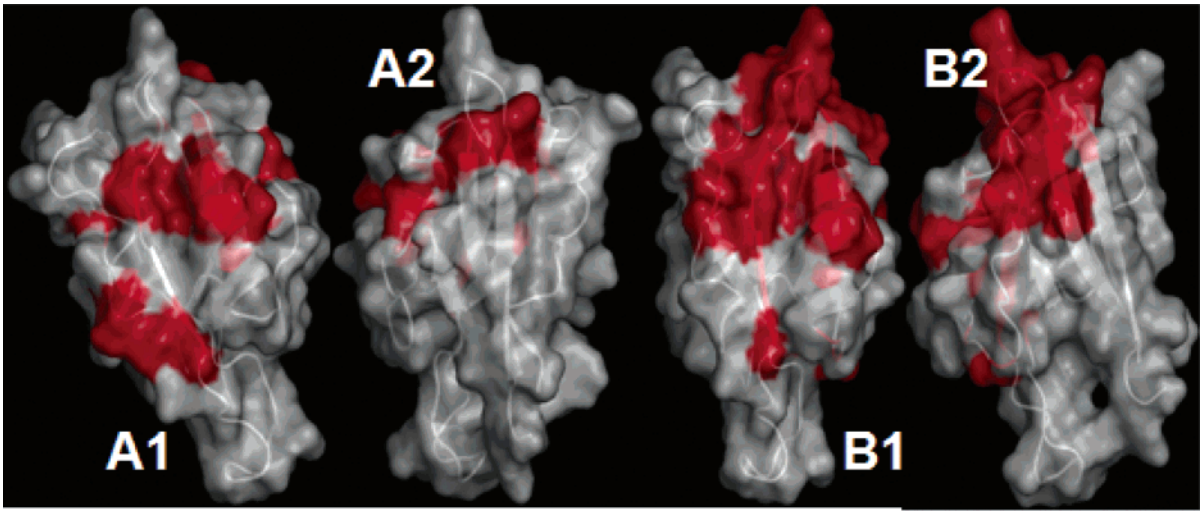

FIGURE 6: Amino acids for which chemical shift changes were identified are mapped on a surface representation of the 3D structure of the neurabin PDZ domain. Differences upon binding of class I or class II peptides are clearly visible and are discussed in detail in the text. A1 and A2 (180° horizontal rotation) map the interaction sites for GluR3-derived peptides and B1 and B2 for NR2A/B-derived peptides on the neurabin PDZ domain.

are the first experimentally identified neuronal class V PDZ domains and therefore are distinct from all other neuronal PDZ domains, such as those from GRIP, PICK, SAP-97, and PSD-95, among others.

A Direct Interaction with NR1C2′ (NMDA) but Not GluR1 (AMPA). Differences in the relative binding affinities of the five C-terminal receptor-derived peptides (GluR2, GluR3, NR1C2′, NR2A/B, and NR2C/D) from those of the spinophilin and neurabin PDZ domains are small, with uniform K_d values between 2 and 10 μM, typical for many PDZ domains. These values were calculated using the NMR-based chemical shift measurements. Differences in the affinities of the different C-terminal peptides can be detected between the neurabin and spinophilin PDZ domains. AMPA receptor-derived peptides exhibit an ~2-fold reduced binding affinity (~10 μM) for the spinophilin PDZ domain when compared to that of the neurabin PDZ domain. We expect this is due to the positively charged lysine residue at position −1 (p^{-1}) in the AMPA receptor-derived peptides that reduces the strength of the interaction because of the more positively charged spinophilin peptide binding pocket. Neurabin's binding pocket is not charged. In contrast, the binding affinities of the NMDA receptor-derived C-terminal peptides are nearly identical between the two PDZ domains.

In addition, the binding of these NMDA class I peptides (NR1C2′, NR2A/B, and NR2C/D) changes the electronic environment of many more residues compared to the AMPA class II-derived peptides (GluR2 and GluR3), as detected by additional chemical shift changes of cross-peaks in 2D $^{1}H-^{15}N$ HSQC spectra. NMDA receptor-derived peptides interact with 28 residues, while AMPA receptor-derived peptides interact with only 14 residues, a key difference in binding and thus likely important for specificity (Figure 6).

In a recent study, Lim et al. (*39*) tested the effect of amino acid substitutions in class I and II peptides on their binding efficiencies. They showed that peptide residues p^0, p^{-2}, and p^{-3} are critical positions for binding affinity, but not the residue at position p^{-1}. In addition, Lim reported that the valine at position p^0 results in a stronger interaction when compared with that of isoleucine and leucine, two other amino acids often found at position p^0. Furthermore, class I peptides that contain threonine at position p^{-2} are superior as binders compared to those containing a serine in this position. Last, peptides containing glutamine or glutamic acid at position p^{-3} are superior binders, closely followed by aspartic acid and serine at position p^{-3}.

In this study, all class I NMDA receptor-derived peptides (valine at position p^0) do bind slightly tighter than AMPA receptor-derived peptides (isoleucine at position p^0) but do have larger interaction surfaces, indicating that valine, most likely because of its smaller size, must fit differently into the peptide binding pocket. This must result in additional interactions formed between the peptide and PDZ domains, necessary for this increased interaction surface. NR1C2′, which has a threonine residue at position p^{-2}, interacts slightly more strongly with the PDZ domains than the NR2A−D-derived peptides, which have a serine at position p^{-2}. This observation is consistent with Lim's observation that class I peptides with Thr at position p^{-2} bind more tightly than those with serine. Finally, the residue at position p^{-3} in all of our proteins is either a glutamic acid or serine. Therefore, on the basis of Lim's results, no significant effect on binding should be exerted by the amino acid at this position.

Valine Is Important for Binding Selectivity. On the basis of our structural results and the peptide binding studies, we find that residue Arg575 (spinophilin) and the corresponding Asn584 (neurabin) play highly critical roles in peptide binding. As stated before, an increased number of residues affected due to NMDA receptor-derived peptide binding and the subsequent changes in their electronic environments can be mapped onto the βA−βB loop, the αB helix, and the loop between αB and βF, all of which are close in space (Figures 2 and 6). What causes these differences in binding interactions for NMDA-derived peptides? On the basis of the study of Lim et al., the peptide residue at position p^0 plays a critical role in this differential behavior. The p^0 residue of the class II AMPA receptor-derived peptides is an isoleucine, while that of the class I NMDA receptor-derived peptides is a valine. Therefore, this single-amino acid

C-terminal change is likely of key importance for the observed differences in their interactions with the neurabin and spinophilin PDZ domains. We feel confident that the carboxyl terminus of the C-terminal valine is capable of forming a H_2O-bridged hydrogen bond with Arg575 (spinophilin) or Asn584 (neurabin) (*40*), while the more bulky isoleucine residue is not capable of forming this hydrogen bond, as reported for other PDZ domain structures. To experimentally verify the importance of the p^0 residue for the differential binding to the neurabin and spinophilin PDZ domain, we designed a class I−class II hybrid peptide, composed of the class II GluR2 peptide backbone (ESVK*X*) with the C-terminal p^0 residue from class I NMDA peptide valine (XXXX*V*) for a hybrid peptide of ESVKV. Indeed, this I to V mutation confers NR binding behavior on the GluR-derived peptide, showing that this binding pattern is strictly regulated by the p^0 residue. This was indicated by a strong change in the chemical shift of the Arg575 (spinophilin) or Asn584 (neurabin) residues following hybrid peptide titration, as only seen before by NR peptides, while also slightly increasing the binding affinity, which would be expected on the basis of Lim's experimental results. Therefore, in spite of the distinct structural differences between the neurabin and the spinophilin PDZ domain, the amino acid composition of the binding peptide, especially the 0 position peptide residue, is critical for binding selectivity.

Differences between Cytosolic Protein−PDZ and Membrane-Bound Receptor−PDZ Domain Interactions. We have also tested binding of the neurabin/spinophilin PDZ domains to two cytosolic protein-derived peptides, a class II C-terminal peptide derived from p70S6 kinase (*4*, *36*) and a class I binding peptide derived from kalirin-7 (*37*). Both of these proteins have been demonstrated to interact with these PDZ domains in vivo. Surprisingly, these peptides have an ∼2−3-fold weaker binding affinity for the PDZ domains than the class I and II receptor-derived peptides (∼30−50 μM). However, even more interesting are the different binding kinetics, which are most pronounced for the p70S6 C-terminal peptide. We are able to detect cross-peaks only in the 2D $^1H-^{15}N$ HSQC spectra when a large surplus of these peptides is used (1:5 and 1:10). For 1:1 and 1:2.5 PDZ domain:peptide molar ratios, we are unable to detect cross-peaks of the interacting residues in the 2D $^1H-^{15}N$ HSQC spectrum. To detect possible errors in the chemical shift measurements, we confirmed the NMR-derived data using ITC measurements (see Table S1 of the Supporting Information). This demonstrates that these cytosolic protein−peptide interactions take place on an intermediate time scale, and their interactions with the neurabin and spinophilin PDZ domains are markedly different from those with the class I and II AMPA/NMDA receptor-derived peptides (fast time scale). In addition, for both peptides, we are able to detect the same interaction pattern as for NMDA receptor-derived peptides, particularly showing a strong chemical shift change for the Arg575/Asn584 residue as described above. This further supports our conclusion that the C-terminal isoleucine of the GluR2/3 peptides, which is different from the valine and leucine (only P70S6 kinase), is the key residue for selectivity. While the underlying biological functions of the cytosolic and membrane-derived proteins are likely equivalent, i.e., targeting PP1 to its points of action, the interaction time scales and complexities between cytosolic- and receptor-derived peptides with these PDZ domains suggest that the mechanism by which this targeting is achieved and regulated is different.

DISCUSSION

PDZ domains are common protein domains which function in protein−protein recognition. PDZ domains typically bind the C-termini of their protein binding partner. This recognition allows multiple proteins to form large macromolecular assemblies, which are vitally important for signaling processes. PDZ domains, until recently, have been categorized into four distinct classes (classes I−IV), which are defined by the canonical sequence of the binding peptides. However, in the past few years, new PDZ domains have been identified that do not fit easily into any of these classes. The neurabin and spinophilin PDZ domain also fall into a new hybrid PDZ class, class V, whose members are able to bind to both class I (E**S**X**V**, where X = D or E) and class II peptides (S**V**K**I**).

By targeting PP1 to the AMPA and NMDA receptors, spinophilin and neurabin regulate the phosphorylation state of these receptors. While the interaction of spinophilin and neurabin with PP1 has been biochemically and physiologically investigated during the past few years, this was not the case for the PDZ domain interactions. It was unknown whether the two proteins target the receptors directly or if additional proteins are used as linking scaffolds. Since PDZ domains are known for their strong interactions with the C-termini from different proteins, especially receptors, we used 5−7-mer peptides, derived from GluR1−4 (AMPA receptors) and NR1, NR2A-D, and NR3 (NMDA receptors), to test for direct interactions with the spinophilin and neurabin PDZ domains. By using 2D $^1H-^{15}N$ HSQC NMR analysis, we were able to demonstrate that both spinophilin and neurabin PDZ domains directly bind to GluR2, GluR3, and NR1C2′-, NR2A/B-, and NR2C/D-derived peptides.

Our peptide binding results show, despite changes in the width of the binding pocket between the neurabin and spinophilin PDZ domain, which is surprising because the sequences of spinophilin and neurabin are 86% identical, the dominant influences on binding selectivity come from the specific amino acid sequence in the C-terminal binding peptides. Notably, NR1C2′-, NR2A/B-, and NR2C/D-derived peptides exhibit interactions with residues outside the major binding pocket (Arg575 in the spinophilin and the corresponding asparagine residue in the neurabin PDZ domain), which seems to effect their interaction in a manner independent of the shape of the binding pocket. Most likely, the carboxyl group of the C-terminal valine fits into the binding pocket and forms a H_2O-mediated hydrogen bond with Arg575 in the spinophilin PDZ domain or the corresponding asparagine residue in the neurabin PDZ domain. The interaction between the peptide and flanking helix αB has been identified as an important element for binding selectivity (*41*). However, despite the differences in the relative angle of helix αB between the spinophilin and neurabin PDZ domain structures, it seems that its spatial orientation does not have an effect on the overall binding affinity of the binding peptides for the PDZ domain.

In neurabin and spinophilin, the PDZ domain is located immediately C-terminal to the PP1-binding domain. The

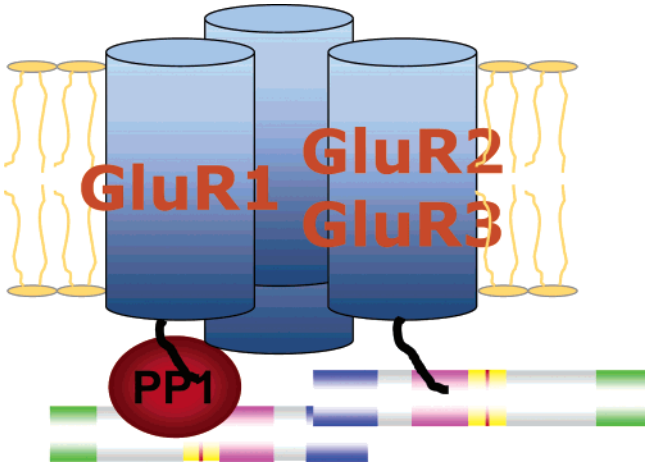

FIGURE 7: Illustration of the spinophilin-mediated PP1 dephosphorylation of the GluR1 AMPA subunit (details in the text).

proximity of these domains may play an important role in directing PP1 toward phosphorylated AMPA and NMDA receptor subunits, thus ensuring maximal catalytic efficiency as well as substrate specificity. Notably, the affinity of neurabin and spinophilin PDZ domains with their glutamate receptor C-terminal peptides was in the low micromolar range. The only moderate affinities of these interactions would enable spinophilin and neurabin to bind to and release from the receptors rapidly, and to allow regulation of glutamate receptor phosphorylation by other signaling pathways, such as when PP1 is inhibited by PKA-phosphorylated DARPP-32 or when the F-actin-binding domain of spinophilin is phosphorylated. By targeting PP1 to glutamate receptors, spinophilin and neurabin have been shown to regulate the phosphorylation state and activity of these channel proteins. Spinophilin and neurabin are highly enriched in dendritic spines by virtue of their interaction with F-actin, and this actin interaction was thought to be largely responsible for directing the actions of PP1 toward its synaptic substrates such as AMPA and NMDA receptors. However, the results of this study suggest that targeting of PP1 toward AMPA and NMDA receptors is also likely to involve direct binding of neurabin and spinophilin with glutamate receptor subunits via PDZ domain−C-termini interactions.

A New Model for AMPA Receptor Dephosphorylation. These data lead to the formulation of a novel model for AMPA receptor dephosphorylation by PP1 (Figure 7). AMPA receptors mediate the majority of fast excitatory transmission, and changes in the efficacy of this transmission underlie plasticity in the CNS. The best-studied form of this plasticity is long-term potentiation (LTP) and long-term depression (LTD). Phosphorylation of AMPA receptor subunits regulates the intrinsic properties of the channel and its interactions with associated proteins. The C-termini of these receptor subunits are especially critical for the regulation of AMPA receptor function. While it is widely recognized that AMPA receptor function is highly complex, including important regulatory effects due to receptor trafficking (*42*, *43*) and interactions with additional membrane proteins, such as stargazin (*44*−*46*), it is evident that the phosphorylation state of Ser845 on GluR1 subunits is one of the most important factors for regulation of AMPA−receptor activity (*47*). For example, using a S845A mutant, it has been shown that phosphorylation of Ser845 results in a dramatic potentiation of channel activity in response to glutamate (*48*).

Low levels of Ser845 phosphorylation directly correlate with low channel open probability and channel trafficking. Other studies have indicated that PP1 is targeted to the AMPA receptor via spinophilin. As our data show, the PDZ domain of spinophilin binds peptides derived from C-termini of GluR2/3 AMPA receptor subunits, but not a peptide from the GluR1 subunit. As previously reported (*36*), proteins such as p70S6 kinase bind only to the PDZ domain of spinophilin/neurabin when PP1 is not bound; i.e., spinophilin/neurabin cannot have the PDZ- and PP1-binding pockets simultaneously occupied. Either intrinsic steric interaction between the spinophilin PP1-binding domain and the PDZ domain or steric blocking when one of the targets, i.e., PP1 or the PDZ domain interaction partner, is bound to spinophilin hinders simultaneous PP1 and PDZ domain binding.

Furthermore, it is known that both spinophilin and neurabin are present as a dimer or higher-order multimeric species in vitro and in vivo. This dimerization is mediated by their coiled-coil domains, domains frequently demonstrated to be important for protein−protein multimerization (*4*, *49*). This dimerization has been shown to be important for regulation of F-actin bundling by neurabin. Spinophilin/neurabin multimerization is mediated by the coiled-coil domain (unpublished data).

Together, our new model predicts that one molecule of spinophilin binds with its PDZ domain to the GluR2/3 subunits of the AMPA receptor and a second spinophilin molecule, which interacts via its coiled-coil domain with the PDZ-bound spinophilin molecule, binds PP1 and targets it to Ser845 of GluR1 (Figure 7). This brings PP1 into the proximity of its point of action, ensuring a high degree of specificity directing PP1 activity toward GluR1. Interaction with NMDA receptors could be mediated by two alternative mechanisms. First, it could follow the same mechanism proposed for AMPA receptor dephosphorylation described above. Alternatively, since we identified a direct interaction with the NR1C2′ subunit, and since simultaneous PDZ and PP1 binding has so far not been demonstrated, a second mechanism would be one in which the first spinophilin molecule binds the NR1C2′ subunit instead of NR2A-D subunits, while the second spinophilin molecule targets PP1 to Ser897 in the NR1 (*50*).

ACKNOWLEDGMENT

W.P. thanks Dr. Rebecca Page for discussion and careful reading of the manuscript and Drs. Dale F. Mierke, Mark Spaller, and John Marshall for discussions.

SUPPORTING INFORMATION AVAILABLE

A figure showing the 3D mapping of the amino acid difference between neurabin and spinophilin on their structures, a figure allowing a visualization of the impact of the single-residue change of I564 (neurabin) to T555 (spinophilin), 2D $^{1}H-^{15}N$ HSQC spectra showing peptide titration results, 2D $^{1}H-^{15}N$ HSQC showing no change upon DMSO titration, and a table showing a comparison between K_d values derived from NMR chemical shifts and ITC measure-

ments. This material is available free of charge via the Internet at http://pubs.acs.org.

REFERENCES

1. Nakanishi, H., Obaishi, H., Satoh, A., Wada, M., Mandai, K., Satoh, K., Nishioka, H., Matsuura, Y., Mizoguchi, A., and Takai, Y. (1997) Neurabin: A novel neural tissue-specific actin filament-binding protein involved in neurite formation, *J. Cell Biol. 139*, 951−961.
2. Allen, P. B., Ouimet, C. C., and Greengard, P. (1997) Spinophilin, a novel protein phosphatase 1 binding protein localized to dendritic spines, *Proc. Natl. Acad. Sci. U.S.A. 94*, 9956−9961.
3. Satoh, A., Nakanishi, H., Obaishi, H., Wada, M., Takahashi, K., Satoh, K., Hirao, K., Nishioka, H., Hata, Y., Mizoguchi, A., and Takai, Y. (1998) Neurabin-II/spinophilin. An actin filament-binding protein with one PDZ domain localized at cadherin-based cell-cell adhesion sites, *J. Biol. Chem. 273*, 3470−3475.
4. Sarrouilhe, D., di Tommaso, A., Metaye, T., and Ladeveze, V. (2006) Spinophilin: From partners to functions, *Biochimie 88*, 1099−1113.
5. Feng, J., Yan, Z., Ferreira, A., Tomizawa, K., Liauw, J. A., Zhuo, M., Allen, P. B., Ouimet, C. C., and Greengard, P. (2000) Spinophilin regulates the formation and function of dendritic spines, *Proc. Natl. Acad. Sci. U.S.A. 97*, 9287−9292.
6. Greengard, P. (2001) The neurobiology of slow synaptic transmission, *Science 294*, 1024−1030.
7. Keegan, J., Schmerer, M., Ring, B., and Garza, D. (2001) The 62E early-late puff of *Drosophila* contains D-spinophilin, an ecdysone-inducible PDZ-domain protein dynamically expressed during metamorphosis, *Genet. Res. 77*, 27−39.
8. Smith, F. D., Oxford, G. S., and Milgram, S. L. (1999) Association of the D2 dopamine receptor third cytoplasmic loop with spinophilin, a protein phosphatase-1-interacting protein, *J. Biol. Chem. 274*, 19894−19900.
9. Wang, X., Zeng, W., Soyombo, A. A., Tang, W., Ross, E. M., Barnes, A. P., Milgram, S. L., Penninger, J. M., Allen, P. B., Greengard, P., and Muallem, S. (2005) Spinophilin regulates Ca^{2+} signalling by binding the N-terminal domain of RGS2 and the third intracellular loop of G-protein-coupled receptors, *Nat. Cell Biol. 7*, 405−411.
10. Yan, Z., Hsieh-Wilson, L., Feng, J., Tomizawa, K., Allen, P. B., Fienberg, A. A., Nairn, A. C., and Greengard, P. (1999) Protein phosphatase 1 modulation of neostriatal AMPA channels: Regulation by DARPP-32 and spinophilin, *Nat. Neurosci. 2*, 13−17.
11. Snyder, G. L., Fienberg, A. A., Huganir, R. L., and Greengard, P. (1998) A dopamine/D1 receptor/protein kinase A/dopamine- and cAMP-regulated phosphoprotein (Mr 32 kDa)/protein phosphatase-1 pathway regulates dephosphorylation of the NMDA receptor, *J. Neurosci. 18*, 10297−10303.
12. Hsieh-Wilson, L. C., Benfenati, F., Snyder, G. L., Allen, P. B., Nairn, A. C., and Greengard, P. (2003) Phosphorylation of spinophilin modulates its interaction with actin filaments, *J. Biol. Chem. 278*, 1186−1194.
13. Hung, A. Y., and Sheng, M. (2002) PDZ domains: Structural modules for protein complex assembly, *J. Biol. Chem. 277*, 5699−5702.
14. Sheng, M., and Sala, C. (2001) PDZ domains and the organization of supramolecular complexes, *Annu. Rev. Neurosci. 24*, 1−29.
15. Jelen, F., Oleksy, A., Smietana, K., and Otlewski, J. (2003) PDZ domains: Common players in the cell signaling, *Acta Biochim. Pol. 50*, 985−1017.
16. Dev, K. K. (2004) Making protein interactions druggable: Targeting PDZ domains, *Nat. Rev. Drug Discovery 3*, 1047−1056.
17. Kim, E., and Sheng, M. (2004) PDZ domain proteins of synapses, *Nat. Rev. Neurosci. 5*, 771−781.
18. Vaccaro, P., Brannetti, B., Montecchi-Palazzi, L., Philipp, S., Helmer Citterich, M., Cesareni, G., and Dente, L. (2001) Distinct binding specificity of the multiple PDZ domains of INADL, a human protein with homology to INAD from *Drosophila melanogaster*, *J. Biol. Chem. 276*, 42122−42130.
19. Vaccaro, P., and Dente, L. (2002) PDZ domains: Troubles in classification, *FEBS Lett. 512*, 345−349.
20. Zhou, H., Xu, Y., Yang, Y., Huang, A., Wu, J., and Shi, Y. (2005) Solution structure of AF-6 PDZ domain and its interaction with the C-terminal peptides from Neurexin and Bcr, *J. Biol. Chem. 280*, 13841−13847.
21. Greengard, P., Allen, P. B., and Nairn, A. C. (1999) Beyond the dopamine receptor: The DARPP-32/protein phosphatase-1 cascade, *Neuron 23*, 435−447.
22. Peti, W., and Page, R. (2007) Strategies to maximize heterologous protein expression in *Escherichia coli* with minimal cost, *Protein Expression Purif. 51*, 1−10.
23. Kelker, M. S., and Peti, W. (2006) NMR assignment of the spinophilin PDZ domain (493−*602), J. Biomol. NMR 36* (Suppl. 5), 24.
24. Sattler, J., Schleucher, J., and Griesinger, C. (1999) Heteronuclear multidimensional NMR experiments for the structure determination of proteins in solution employing pulsed field gradients, *Prog. NMR Spectrosc. 34*, 93−158.
25. Herrmann, T., Güntert, P., and Wüthrich, K. (2002) Protein NMR structure determination with automated NOE assignment using the new software CANDID and the torsion angle dynamics algorithm DYANA, *J. Mol. Biol. 319*, 209−227.
26. Herrmann, T., Güntert, P., and Wüthrich, K. (2002) Protein NMR structure determination with automated NOE-identification in the NOESY spectra using the new software ATNOS, *J. Biomol. NMR 24*, 171−189.
27. Güntert, P. (2004) Automated NMR Structure Calculation With CYANA, *Methods Mol. Biol. 278*, 353−378.
28. Peti, W., Etezady-Esfarjani, T., Herrmann, T., Klock, H. E., Lesley, S. A., and Wüthrich, K. (2004) NMR for structural proteomics of *Thermotoga maritima*: Screening and structure determination, *J. Struct. Funct. Genomics 5*, 205−215.
29. Peti, W., Herrmann, T., Zagnitko, O., Grzechnik, S. K., and Wüthrich, K. (2005) NMR structure of the conserved hypothetical protein TM0979 from *Thermotoga maritima*, *Proteins 59*, 387−390.
30. Peti, W., Johnson, M. A., Herrmann, T., Neuman, B. W., Buchmeier, M. J., Nelson, M., Joseph, J., Page, R., Stevens, R. C., Kuhn, P., and Wüthrich, K. (2005) Structural genomics of the severe acute respiratory syndrome coronavirus: Nuclear magnetic resonance structure of the protein nsP7, *J. Virol. 79*, 12905−12913.
31. Nederveen, A. J., Doreleijers, J. F., Vranken, W., Miller, Z., Spronk, C. A., Nabuurs, S. B., Güntert, P., Livny, M., Markley, J. L., Nilges, M., Ulrich, E. L., Kaptein, R., and Bonvin, A. M. (2005) RECOORD: A recalculated coordinate database of 500+ proteins from the PDB using restraints from the BioMagResBank, *Proteins 59*, 662−672.
32. Brünger, A. T., Adams, P. D., Clore, G. M., DeLano, W. L., Gros, P., Grosse-Kunstleve, R. W., Jiang, J. S., Kuszewski, J., Nilges, M., Pannu, N. S., Read, R. J., Rice, L. M., Simonson, T., and Warren, G. L. (1998) Crystallography & NMR system: A new software suite for macromolecular structure determination, *Acta Crystallogr. D54* (Part 5), 905−921.
33. Hooft, R. W., Vriend, G., Sander, C., and Abola, E. E. (1996) Errors in protein structures, *Nature 381*, 272.
34. Laskowski, R. A., Rullmannn, J. A., MacArthur, M. W., Kaptein, R., and Thornton, J. M. (1996) AQUA and PROCHECK-NMR: Programs for checking the quality of protein structures solved by NMR, *J. Biomol. NMR 8*, 477−486.
35. Koradi, R., Billeter, M., and Wüthrich, K. (1996) MOLMOL: A program for display and analysis of macromolecular structures, *J. Mol. Graphics 14*, 51−55, 29−32.
36. Burnett, P. E., Blackshaw, S., Lai, M. M., Qureshi, I. A., Burnett, A. F., Sabatini, D. M., and Snyder, S. H. (1998) Neurabin is a synaptic protein linking p70 S6 kinase and the neuronal cytoskeleton, *Proc. Natl. Acad. Sci. U.S.A. 95*, 8351−8356.
37. Penzes, P., Johnson, R. C., Sattler, R., Zhang, X., Huganir, R. L., Kambampati, V., Mains, R. E., and Eipper, B. A. (2001) The neuronal Rho-GEF Kalirin-7 interacts with PDZ domain-containing proteins and regulates dendritic morphogenesis, *Neuron 29*, 229−242.
38. McGuffin, L. J., Bryson, K., and Jones, D. T. (2000) The PSIPRED protein structure prediction server, *Bioinformatics 16*, 404−405.
39. Lim, I. A., Hall, D. D., and Hell, J. W. (2002) Selectivity and promiscuity of the first and second PDZ domains of PSD-95 and synapse-associated protein 102, *J. Biol. Chem. 277*, 21697−21711.
40. Harris, B. Z., and Lim, W. A. (2001) Mechanism and role of PDZ domains in signaling complex assembly, *J. Cell Sci. 114*, 3219−3231.
41. Songyang, Z., Fanning, A. S., Fu, C., Xu, J., Marfatia, S. M., Chishti, A. H., Crompton, A., Chan, A. C., Anderson, J. M., and Cantley, L. C. (1997) Recognition of unique carboxyl-terminal motifs by distinct PDZ domains, *Science 275*, 73−77.

42. Kennedy, M. J., and Ehlers, M. D. (2006) Organelles and trafficking machinery for postsynaptic plasticity, *Annu. Rev. Neurosci. 29*, 325−362.
43. Nicoll, R. A., Tomita, S., and Bredt, D. S. (2006) Auxiliary subunits assist AMPA-type glutamate receptors, *Science 311*, 1253−1256.
44. Vandenberghe, W., Nicoll, R. A., and Bredt, D. S. (2005) Stargazin is an AMPA receptor auxiliary subunit, *Proc. Natl. Acad. Sci. U.S.A. 102*, 485−490.
45. Priel, A., Kolleker, A., Ayalon, G., Gillor, M., Osten, P., and Stern-Bach, Y. (2005) Stargazin reduces desensitization and slows deactivation of the AMPA-type glutamate receptors, *J. Neurosci. 25*, 2682−2686.
46. Tomita, S., Sekiguchi, M., Wada, K., Nicoll, R. A., and Bredt, D. S. (2006) Stargazin controls the pharmacology of AMPA receptor potentiators, *Proc. Natl. Acad. Sci. U.S.A. 103*, 10064−10067.
47. Roche, K. W., O'Brien, R. J., Mammen, A. L., Bernhardt, J., and Huganir, R. L. (1996) Characterization of multiple phosphorylation sites on the AMPA receptor GluR1 subunit, *Neuron 16*, 1179−1188.
48. Banke, T. G., Bowie, D., Lee, H., Huganir, R. L., Schousboe, A., and Traynelis, S. F. (2000) Control of GluR1 AMPA receptor function by cAMP-dependent protein kinase, *J. Neurosci. 20*, 89−102.
49. Mason, J. M., and Arndt, K. M. (2004) Coiled coil domains: Stability, specificity, and biological implications, *ChemBioChem 5*, 170−176.
50. Dudman, J. T., Eaton, M. E., Rajadhyaksha, A., Macias, W., Taher, M., Barczak, A., Kameyama, K., Huganir, R., and Konradi, C. (2003) Dopamine D1 receptors mediate CREB phosphorylation via phosphorylation of the NMDA receptor at Ser897-NR1, *J. Neurochem. 87*, 922−934.
51. Korzhnev, D. M., Billeter, M., Arseniev, A. S., and Orekhov, V. Y. (2001) NMR studies of Brownian tumbling and internal motions in proteins, *Prog. Nucl. Magn. Reson. Spectrosc. 38*, 197−266.
52. Fischer, M. W. F., Majumdar, A., and Zuiderweg, E. R. P. (1998) Protein NMR relaxation: Theory, applications and outlook, *Prog. Nucl. Magn. Reson. Spectrosc. 33*, 207−272.
53. DeLano, W. L. (2002) *PyMOL*, DeLano Scientific LLC, San Carlos, CA.

BI602341C